



## Customizing speckle intensity statistics

NICHOLAS BENDER,<sup>1</sup> HASAN YILMAZ,<sup>1</sup>  YARON BROMBERG,<sup>2</sup> AND HUI CAO<sup>1,\*</sup>

<sup>1</sup>Department of Applied Physics, Yale University, New Haven, Connecticut 06520, USA

<sup>2</sup>Racah Institute of Physics, The Hebrew University of Jerusalem, Jerusalem 91904, Israel

\*Corresponding author: hui.cao@yale.edu

Received 9 February 2018; revised 6 April 2018; accepted 7 April 2018 (Doc. ID 322894); published 9 May 2018

**Speckles commonly satisfy Rayleigh statistics. However, in many applications, non-Rayleigh speckles with customized intensity statistics are desirable. Here, we present a general method for customizing the intensity statistics of speckle patterns on a target plane. By judiciously modulating the phase front of a monochromatic laser beam, we experimentally generate speckle patterns with arbitrarily tailored intensity probability density functions. Relative to Rayleigh speckles, our customized speckles exhibit radically different topologies yet maintain the same spatial correlation length. The customized speckles are fully developed, ergodic, and stationary—with circular non-Gaussian statistics for the complex field. Propagating away from the target plane, the customized speckles revert back to Rayleigh speckles. This work provides a versatile framework for tailoring speckle patterns with varied applications in microscopy, imaging, and optical manipulation.** © 2018 Optical Society of America under the terms of the [OSA Open Access Publishing Agreement](#)

**OCIS codes:** (030.0030) Coherence and statistical optics; (030.6140) Speckle; (030.6600) Statistical optics.

<https://doi.org/10.1364/OPTICA.5.000595>

### 1. INTRODUCTION

Speckle formation is a phenomenon inherent to both classical and quantum waves. Characterized by a random granular structure, a speckle pattern arises when a coherent wave undergoes a disorder-inducing scattering process. The statistical properties of a speckle pattern are generally universal—commonly referred to as Rayleigh statistics—featuring a circular Gaussian distribution for the complex-field joint probability density function (PDF), and a negative-exponential intensity PDF [1–4]. Typically, non-Rayleigh speckles are classified as either under-developed (sum of a small number of scattered waves or the phase of these waves not fully randomized) or partially coherent (sum of incoherent partial waves) [5–13]. In both cases, the diversity of the intensity PDF's functional form is limited.

There has been a plethora of interest in creating speckle patterns with tailored statistics [14–23], due to their potential applications in structured-illumination imaging: for example, dynamic speckle illumination microscopy [24,25], super-resolution imaging [26,27], and pseudo-thermal light sources for high-order ghost imaging [28–30]. Furthermore, a general method for customizing both the statistics and topology of laser speckle patterns would be a valuable tool for synthesizing optical potentials for cold atoms [31], microparticles [32–35], and active media [36–38].

Recently, a simple method was developed for creating non-Rayleigh speckle patterns with a phase-only spatial light modulator (SLM) [17]. High-order correlations were encoded into the field by the SLM, leading to a redistribution of the light intensity among the speckle grains in the far field. In this method,

the speckle pattern could possess an intensity PDF with a tail decaying either slower or faster than a negative-exponential function. It was not known, however, if it was possible to have an intensity PDF of any functional form, such as increasing with intensity, or double-peaked at specific values.

In this work, we present a general method for tailoring the intensity statistics of speckle patterns by modulating the phase front of a laser beam with a SLM. Starting with a Rayleigh speckle pattern, we numerically apply a local intensity transformation to obtain a new speckle pattern that is governed by a target PDF. Subsequently, this pattern is generated experimentally in the far field of the SLM, where the requisite phase modulation is determined numerically via a nonlinear optimization algorithm. Via this process, we can create speckle patterns governed by arbitrary intensity PDFs—within a predefined intensity range of interest. Such speckle patterns exhibit distinct topologies relative to Rayleigh speckles, but retain the same spatial correlation length. A thorough study of the statistical properties reveals that the speckles are of a new kind—that has not been reported before. Despite being fully developed, ergodic, and stationary, the joint complex-field PDFs of the speckle patterns are circular non-Gaussian, with higher-order intensity moments differing from those of Rayleigh speckles. Both intensity statistics and speckle topology evolve with beam propagation away from the target plane, wherein the speckle patterns eventually revert back to Rayleigh speckles. This work provides a versatile framework for customizing speckle patterns for varied applications in microscopy, imaging, and optical manipulation.

## 2. EXPERIMENTAL SETUP AND METHOD

In our experiment, a reflective, phase-only SLM (Hamamatsu LCoS X10468) is illuminated with a linearly polarized monochromatic laser beam at a wavelength of  $\lambda = 642$  nm (Coherent OBIS). The laser beam is expanded and clipped by an iris to uniformly illuminate the phase modulation region of the SLM. The central part of the phase modulation region of the SLM is partitioned into a square array of  $32 \times 32$  macropixels, each consisting of  $16 \times 16$  pixels. The remaining illuminated pixels outside the central square diffract the laser beam away from the target plane via a phase grating. The SLM is placed at the front focal plane of a lens,  $f = 500$  mm, and the intensity pattern at the back focal plane is recorded with a charge-coupled device (CCD) camera (Allied Vision Prosilica GC660). The laser beam incident upon the SLM is linearly polarized, and the incident angles on the camera are too small to introduce a significant polarization component in the axial direction. Thus, the light waves incident on the camera can be modeled as scalar waves. To a good approximation, the field pattern on the camera chip is a Fourier transform of the field of the SLM's surface.

Next we describe how to determine a target speckle intensity pattern governed by an arbitrary intensity PDF. When a Gaussian random phase pattern is displayed on the SLM, the intensity pattern recorded by the camera is a Rayleigh speckle pattern, as shown in Fig. 1(a). We numerically perform a local intensity transformation on a recorded Rayleigh speckle pattern, which converts it into a speckle intensity pattern governed by the desired PDF  $F(\tilde{I})$ . The intensity PDF of the Rayleigh speckle pattern,  $P(I) = \exp[-I/\langle I \rangle]/\langle I \rangle$ , can be related to the target PDF  $F(\tilde{I})$  by

$$P(I)dI = F(\tilde{I})d\tilde{I}. \quad (1)$$

This relation is the starting point for determining the local intensity transformation  $\tilde{I} = f(I)$ , which is applied to the intensity values of a Rayleigh speckle pattern to create a new speckle pattern with the desired PDF. To solve for the specific intensity

transformation associated with the PDF  $F(\tilde{I})$ , we write Eq. (1) in integral form with  $\langle I \rangle = 1$ :

$$\int_0^I e^{-I'} dI' = \int_{\tilde{I}_{\min}}^{\tilde{I}} F(\tilde{I}') d\tilde{I}'. \quad (2)$$

Evaluating the integrals and solving for  $\tilde{I}$  as a function of  $I$  gives the desired local intensity transformation  $\tilde{I} = f(I)$ . In addition to altering the intensity PDF, such a transformation provides the freedom to regulate the maximum or minimum intensity values of the transformed pattern. We may arbitrarily set  $\tilde{I}_{\max}$  or  $\tilde{I}_{\min}$ , as long as the following normalization conditions hold:  $\int_{\tilde{I}_{\min}}^{\tilde{I}_{\max}} F(\tilde{I}') d\tilde{I}' = 1$  and  $\langle \tilde{I} \rangle = \int_{\tilde{I}_{\min}}^{\tilde{I}_{\max}} \tilde{I}' F(\tilde{I}') d\tilde{I}' = \langle I \rangle$ . Such regulatory ability is useful for practical applications such as speckle illumination, where without altering the total power of illumination, the maximal intensity value can be set below the damage threshold of a sample or the minimum intensity value can be set to exceed the noise floor.

The local intensity transformation is typically nonlinear and therefore produces spatial frequency components that are higher than those in the original pattern—and therefore outside the range of spatial frequencies accessible in the experiment. Nevertheless, these components can be removed from the intensity pattern by applying a digital low-pass Fourier filter—where the allowed frequency window is a square. The high frequency cutoff of the filter is determined by the average value of the maximum spatial-frequency component present in the Rayleigh speckle patterns generated by our setup. The resulting filtered pattern will, however, have an intensity PDF  $\tilde{F}(\tilde{I})$  slightly deviating from the target one,  $F(\tilde{I})$ . Such deviations can be eliminated by applying an additional intensity transformation  $\tilde{I} = \tilde{f}(\tilde{I})$  that is obtained from  $\int_{\tilde{I}_{\min}}^{\tilde{I}} \tilde{F}(\tilde{I}') d\tilde{I}' = \int_{\tilde{I}_{\min}}^{\tilde{I}} F(\tilde{I}') d\tilde{I}'$ . The process of performing a local intensity transformation, and subsequently applying a digital low-pass Fourier filter, can be repeated iteratively as the conventional Gerchberg–Saxton method [39] until the target PDF is obtained for a speckle pattern obeying the spatial-frequency restrictions. Repetition of this procedure with different initial Rayleigh

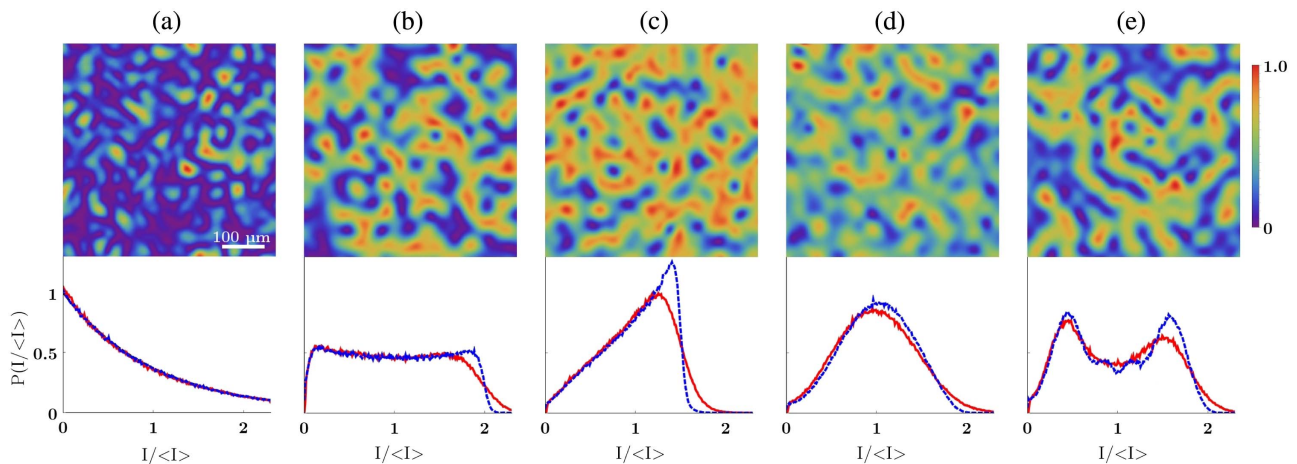


**Fig. 1.** (a) Rayleigh speckle pattern and (b–e) customized speckle patterns with distinct intensity statistics. In the top row, each pattern has a size of  $504 \mu\text{m}$  by  $504 \mu\text{m}$ , and the maximum intensity is normalized to 1. The associated PDF, shown in the lower row, is (b) uniform, (c) increasing linearly, (d) peaked at a non-zero intensity, and (e) bimodal, within a predefined range of intensity. The red solid curves are experimental data, whereas the blue dashed curves are from numerically generated target speckle patterns. Both are a result of spatial and ensemble averaging over 50 independent speckle patterns.

speckles creates a set of independent intensity patterns that possesses the same PDFs. It is important to note, however, that certain PDFs cannot be generated in our experiment because of the finite range of spatial frequencies (see Supplement 1 for more details).

Having created intensity patterns with the desired PDF, the next step is to determine the phase pattern on the SLM to generate the target pattern on the camera. Assuming the SLM consists of an  $N \times N$  array of macropixels, a discrete Fourier transform gives an  $N \times N$  array of independent elements, each representing a speckle grain. To avert the effects of aliasing and uniquely define the spatial profile measured by the camera, it is necessary to sample the speckle pattern at or above the Nyquist limit. This means every speckle grain should be sampled at least twice along each spatial axis. Thus, the  $N \times N$  speckles generated on the camera chip must be sampled by at least  $2N \times 2N$  points. We note that the  $2N \times 2N$  intensity array contains correlations between adjacent elements.

Because the phases on the SLM are transcendently related to the intensity values on the Fourier plane, there is no closed-form solution for the  $N^2$  independent phases of the SLM macropixels to generate the  $4N^2$  partially correlated intensity values of the target speckle pattern. Thus, we have to find the solution numerically. To facilitate the convergence to a numerical solution, we reduce the controlled area in the camera plane to the central quarter of  $N^2$ , denoted the target region, and neglect the remaining three quarters, denoted the buffer zone. Experimentally, we record the speckle pattern well above the Nyquist limit with the CCD camera:  $\sim 10$  camera pixels per speckle grain along each axis. Such over-sampling does not affect the solution due to spatial correlations within individual speckle grains.

Experimentally, the Fourier relation between the field reflected off the SLM and that in the camera plane is only approximate, and we characterize the precise relation by measuring the field transmission matrix (T-matrix). In addition to encapsulating the experimental imperfections induced by optical misalignment–SLM surface curvature, lens aberrations, and the non-uniform laser illumination of the SLM—employing the transmission matrix provides a general formalism that can be adapted to other setups (e.g., holographic optical tweezers [40]) or to tailor the speckle statistics at a plane other than the Fourier plane. In this work, the T-matrix is measured by a common path interference method akin to those in [41–43]. Briefly, the phase modulation region of the SLM is divided into two equal parts. We sequentially display a series of orthogonal phase patterns on one part while keeping the phase pattern on the other part fixed. Simultaneously, we record the resulting interference patterns on the camera. Subsequent to this, we exchange the role of each part and repeat the measurement. Using all the interference patterns, we can construct a linear mapping between the field on the SLM and the field on the camera—the T-matrix. The measured T-matrix deviates only slightly from a discrete Fourier transform. Using the measured T-matrix, we find the requisite phase pattern on the SLM with a nonlinear optimization algorithm [44,45]. Numerically, we minimize the difference between the target intensity pattern and the pattern obtained by applying the T-matrix to the SLM phase array. Starting with the SLM phase pattern that generates the original Rayleigh speckle, the algorithm converges to a solution for the SLM phase array that generates a given intensity pattern in the target region of the camera plane.

### 3. CUSTOMIZED SPECKLE PATTERNS

Examples of experimentally generated speckle patterns with customized intensity statistics are shown in Figs. 1(b)–1(e), with  $\langle I \rangle$  normalized to 1. In Fig. 1(b), the speckle pattern was designed to have a uniform intensity PDF, over the predefined intensity range of  $I = 0$  and 2. This example illustrates that it is possible to create speckle patterns with non-decaying PDFs in addition to confining the speckle intensities within a finite range. Taking this one step further in Fig. 1(c), we first make the PDF increase linearly with intensity  $P(I) = I$ , and then have it drop rapidly to 0 above the specified threshold of  $I = \sqrt{2}$ . To demonstrate that our method is not restricted to monotonic functions, in Fig. 1(d) we create a speckle pattern with a unimodal intensity PDF given by  $\sin[(\frac{\pi}{2})I]^2$  between  $I_{\min} = 0$  and  $I_{\max} = 2$ . To further increase the complexity of the speckle statistics, Fig. 1(e) shows an example of a bimodal PDF (see Supplement 1 for more information).

In all cases, the experimentally generated speckle patterns possess intensity PDFs that follow the target functional form over the intensity ranges of interest and converge to 0, quickly, outside. Small deviations between the experimental PDFs and the target ones are caused by error in the T-matrix measurement due to experimental noise and temporal decorrelations. We modeled these effects and numerically reproduced the deviations (see Supplement 1 for a full description of our model). Our model describes why the deviations are stronger at higher intensity values or where the PDF varies rapidly with intensity.

Additionally, Fig. 1 illustrates how the topology of the customized speckle patterns changes in accordance with the PDF. The spatial intensity profile of a Rayleigh speckle pattern in Fig. 1(a) can be characterized as a random interconnected web of dark channels surrounding bright islands. Conversely, for speckles with a linearly increasing PDF in Fig. 1(c), the spatial intensity profile is an interwoven web of bright channels with randomly dispersed dark islands. Similarly, the spatial structure of speckles with a bimodal PDF in Fig. 1(e) consists of interlaced bright and dim channels. The topological changes in the customized speckles result from the local intensity transformation and digital low-pass Fourier filtering (see Supplement 1 for details). The continuous network of high intensity in the customized speckle pattern, which is absent in the Rayleigh speckle pattern, will be useful for controlling the transport of trapped atoms or microparticles in optical potentials.

### 4. STATISTICAL PROPERTIES OF CUSTOMIZED SPECKLE PATTERNS

In this section, we analyze the statistical properties of the customized speckle patterns to illustrate their stark difference relative to previously studied speckles.

We start by verifying that the speckle patterns are fully developed and the phase distribution  $\Phi(\theta)$  of the generated speckle fields is uniform over a range of  $2\pi$ . To find  $\Phi(\theta)$ , we use the measured transmission matrix and the SLM phase patterns to recover the fields associated with the intensity patterns recorded by the CCD camera. Figure 2(a) plots  $\Phi(\theta)$  in the target region for the four customized PDFs shown in Fig. 1(b)–1(e), in addition to the case of a Rayleigh PDF. All cases have nearly constant values over  $[0, 2\pi]$ , and, thus, our speckle patterns are fully developed. This property differentiates our speckle patterns with

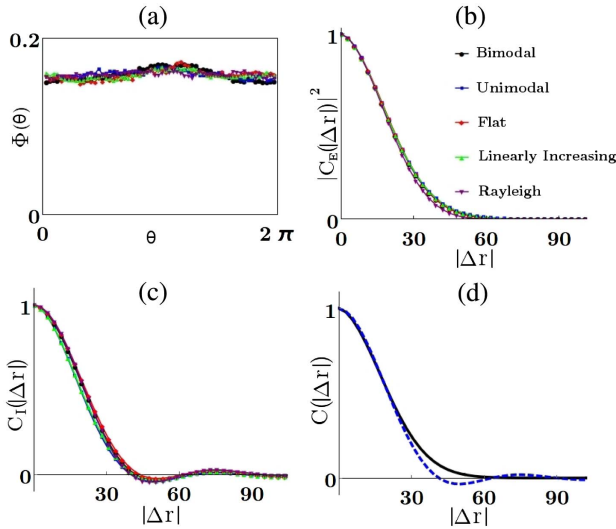


**Fig. 2.** Characteristics of customized speckle patterns. (a) The phase histogram of the speckle fields demonstrates that they are all fully developed speckles. (b) The spatial field correlation function,  $|C_E(\Delta\mathbf{r})|^2$ , and (c) the spatial intensity correlation function,  $C_I(\Delta\mathbf{r})$ , for the customized speckles, remain the same as in Rayleigh speckles. In panels (a–c), the four customized speckle patterns have constant (black), linearly increasing (red), unimodal (blue), and bimodal (green) PDFs, and the purple is for Rayleigh speckles. (d) Comparing  $|C_E(\Delta\mathbf{r})|^2$  (black curve) to  $C_I(\Delta\mathbf{r})$  (blue dashed curve), both averaged over the five curves in (b) and (c), respectively, to confirm that they have the same correlation width.

a unimodal PDF, shown in Fig. 1(d), from partially developed speckle patterns that possess a similar intensity PDF [2].

Next, we check whether additional spatial correlations are introduced into the customized speckle patterns, relative to Rayleigh speckles. To this end, we calculate the 2D spatial correlation function of the speckle field:  $C_E(\Delta\mathbf{r}) = \langle \tilde{E}(\mathbf{r})\tilde{E}^*(\mathbf{r} + \Delta\mathbf{r}) \rangle / \langle \tilde{I} \rangle$ . As shown in Fig. 2(b), the customized speckles have a similar field correlation function as a Rayleigh speckle pattern. This means the way we tailor the speckle statistics does not affect the spatial field correlation function. Furthermore, the 2D spatial intensity correlation function,  $C_I(\Delta\mathbf{r}) = (\langle \tilde{I}(\mathbf{r})\tilde{I}(\mathbf{r} + \Delta\mathbf{r}) \rangle - \langle \tilde{I} \rangle^2) / (\langle \tilde{I}^2 \rangle - \langle \tilde{I} \rangle^2)$ , plotted in Fig. 2(c) for the four customized speckles, has the same width as a Rayleigh speckle pattern. Hence, we can manipulate the speckle intensity PDF without altering the spatial correlation length.

Similarly to the Rayleigh speckles, the customized speckle patterns have the same width for  $\langle |C_E(\Delta\mathbf{r})|^2 \rangle$  and  $\langle C_I(\Delta\mathbf{r}) \rangle$ , as shown in Fig. 2(d). Relative to  $\langle |C_E(\Delta\mathbf{r})|^2 \rangle$ , however,  $\langle C_I(\Delta\mathbf{r}) \rangle$  exhibits small oscillations on the tail. These are attributed to the low-pass Fourier filtering of the intensity pattern, which we use to remove the high-spatial-frequency components introduced during the nonlinear transformation of a Rayleigh speckle pattern. For confirmation of this, we applied the digital low-pass Fourier filter to Rayleigh speckle patterns and the same oscillations appeared in the spatial intensity correlation function, shown in Fig. 2(c).

Now we investigate whether the generation of tailored speckle patterns can be described statistically as a stationary and ergodic process. For a target intensity PDF, we numerically create 2500 speckle patterns consisting of 2500 speckle grains each. Figure 2(a) and 2(b) shows the results for the bimodal PDF.

In Fig. 2(a), the intensity PDF obtained for each of the 2500 ensembles is invariant as a function of ensembles, indicating the speckle patterns are stationary. In Fig. 2(b), the ensemble-averaged intensity PDF for individual spatial positions in the speckle patterns is also invariant as a function of spatial position and is statistically identical to Fig. 2(a), demonstrating the ergodicity of the speckle patterns.

Figure 3(c) shows that the joint complex-field PDF of the bimodal speckles is circular non-Gaussian, in contrast to the circular Gaussian PDF of Rayleigh speckles. Circularity reflects the fact that the amplitude and phase of the speckle field  $E$ —at a single point in space—are uncorrelated [2,4]. Figure 3(d) shows the joint PDF  $P(I_1, I_2)$  for two speckle intensities at locations separated by more than the average speckle grain size. Because  $P(I_1, I_2) = P(I_1)P(I_2)$  (see Supplement 1), the two intensities are statistically independent, which is consistent with the spatial correlation length of speckle intensity. The other types of customized speckle patterns display similar characteristic, and the results are presented in Supplement 1.

The non-Gaussian statistics of the tailored speckle patterns also emerge in their high-order intensity moments,  $\langle I^n \rangle = \int_0^\infty I^n P(I) dI$ , which differ from those of Rayleigh speckles—shown in Table 1. For the case of Rayleigh speckles generated by a Gaussian-random process, the high-order moments are related by  $\langle I^n \rangle = n! \langle I \rangle^n$  [3]. For the customized speckles,  $\langle I^n \rangle$  deviates from  $n! \langle I \rangle^n$ , because of high-order correlations among the partial waves that generate these patterns [17].

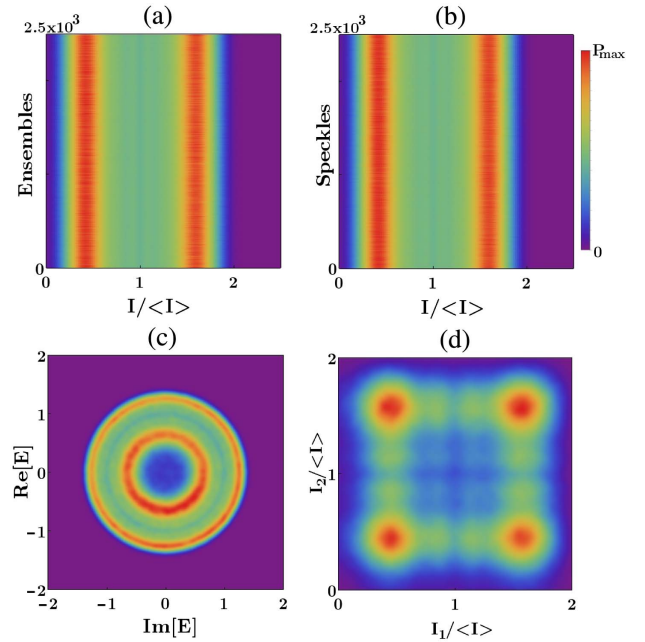


**Fig. 3.** Statistical properties of the customized speckle patterns with a bimodal intensity PDF. (a) The spatially averaged intensity PDF,  $P_S(I)$ , of 2500 speckle patterns verifies that the speckle patterns are stationary. (b) The ensemble-averaged intensity PDF,  $P_E(I)$ —within the area of a single speckle grain—for each spatial position in a pattern confirms that the speckles are ergodic. (c) The complex-amplitude joint PDF for the speckle field,  $P(\text{Re}[E], \text{Im}[E])$ , displays circular non-Gaussian statistics. (d) The joint PDF for two intensities,  $P(I_1, I_2)$ , at spatial positions separated by approximately one speckle grain size (twice the spatial intensity correlation width) are uncorrelated. The results in panels (c, d) are obtained from averaging over space and 100 speckle patterns; a digital low-pass Fourier filter is applied to remove noise.

**Table 1. Intensity Moments of Speckle Patterns with Different Intensity PDFs**

PDF	$\langle I \rangle$	$\langle I^2 \rangle$	$\langle I^3 \rangle$	$\langle I^4 \rangle$	$\langle I^5 \rangle$	$\langle I^6 \rangle$
Negative Exponential	1.00	2.00	6.00	24.0	120	720
Constant	1.00	1.35	2.06	3.39	5.87	10.51
Linearly Increasing	1.00	1.16	1.45	1.92	2.64	3.77
Unimodal	1.00	1.18	1.55	2.22	3.40	5.50
Bimodal	1.00	1.29	1.9	2.99	4.93	8.42

**5. AXIAL PROPAGATION**

Finally, we study how the tailored speckle patterns evolve as they propagate axially. Our method gives the target PDF for speckle patterns on the Fourier plane of the SLM. Outside of the Fourier plane, however, the intensity statistics and topology may change. In the case of a Rayleigh speckle pattern, the spatial pattern changes upon propagation, whereas the intensity PDF remains a negative exponential. We define  $R_l$  as the axial correlation length of the intensity pattern, which corresponds to the Rayleigh range and gives the longitudinal length of a single speckle grain.

The top row in Fig. 4 shows the axial evolution of speckles that have a linearly increasing PDF at the Fourier plane  $z = 0$  [Fig. 4(a)]. As the speckle pattern propagates to  $z = R_l/5$ , the PDF becomes bell-shaped [Fig. 4(b)]. With further propagation,

the maximum of the PDF migrates to a smaller intensity value, as shown in Fig. 4(c) for  $z = (2/5)R_l$ , until it reaches  $I = 0$ . The speckles revert to Rayleigh statistics at  $z \approx R_l$ , beyond which the PDF maintains a negative exponential, as shown in Fig. 4(d) for  $z = (10/7)R_l$ . The topology of the speckle pattern evolves together with the intensity PDF: the interconnected web of bright channels first attenuates upon propagation, and then breaks into islands with dark channels forming.

In Fig. 4(e)–4(f), we show the axial evolution of a speckle pattern with a bimodal PDF at  $z = 0$  [Fig. 4(e)]. As the pattern propagates to  $z = R_l/5$  in Fig. 4(f), the peaks are eroded asymmetrically, with the high-intensity peak diminishing first. Further propagation to  $z = (2/5)R_l$  results in a unimodal PDF [Fig. 4(g)]. Once the axial distance  $z$  exceeds  $R_l$ , the speckles return to Rayleigh statistics, as shown in Fig. 4(h) for  $z = (10/7)R_l$ . A corresponding change of speckle topology is seen: the bright channels disappear first, and then the dim channels fracture, while neighboring dark islands merge to form channels. Therefore, axial propagation, within the range of  $R_l$ , alters the intensity PDF functional form and the speckle topology.

**6. CONCLUSION**

In conclusion, we have presented a general method for customizing speckle intensity statistics using a phase-only

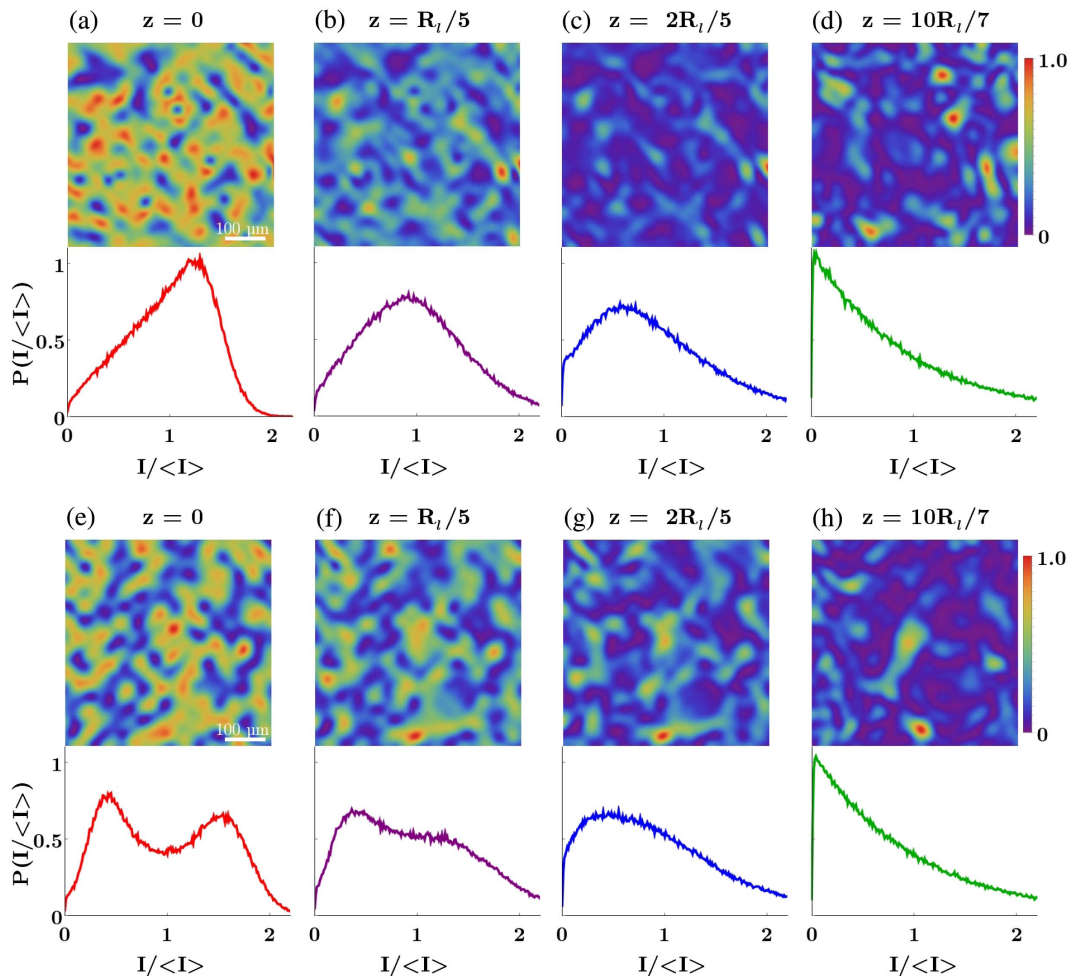


**Fig. 4.** Evolution of customized speckle patterns upon axial propagation. The intensity PDF at the Fourier plane of the SLM ( $z = 0$ ) is (a) increasing linearly and (e) bimodal. The distance from the Fourier plane is (b, f)  $R_l/5$ , (c, g)  $(2/5)R_l$ , and (d, h)  $(10/7)R_l$ .

SLM. The generated speckle patterns possess radically different intensity PDFs and topology relative to Rayleigh speckles. However, they are fully developed speckles that maintain the basic characteristics of stationarity and ergodicity. Their unusual statistical properties engender a new type of speckle pattern with non-Gaussian statistics. Our method is versatile and compatible with a broad range of optical setups. Given the plethora of potential applications, it paves the way for new directions in both fundamental research (many-body physics in random optical potentials with tailored statistics) and applied research (speckle-illumination-based imaging and speckle optical tweezers).

**Funding.** Office of Naval Research (ONR) (N00014-13-1-0649).

**Acknowledgment.** We thank Chia Wei Hsu and Owen Miller for useful discussions.

See [Supplement 1](#) for supporting content.

## REFERENCES AND NOTES

- J. W. Goodman, "Some fundamental properties of speckle," *J. Opt. Soc. Am.* **66**, 1145–1150 (1976).
- J. W. Goodman, *Speckle Phenomena in Optics: Theory and Applications* (Roberts and Company, 2007).
- J. C. Dainty, "An introduction to 'Gaussian' speckle," *Proc. SPIE* **243**, 2–8 (1980).
- J. C. Dainty, *Laser Speckle and Related Phenomena*, Topics in Applied Physics (Springer, 2013).
- J. C. Dainty, "Some statistical properties of random speckle patterns in coherent and partially coherent illumination," *J. Mod. Opt.* **17**, 761–772 (1970).
- B. M. Levine and J. C. Dainty, "Non-Gaussian image plane speckle: measurements from diffusers of known statistics," *Opt. Commun.* **45**, 252–257 (1983).
- J. W. Goodman, "Dependence of image speckle contrast on surface roughness," *Opt. Commun.* **14**, 324–327 (1975).
- H. Fujii and T. Asakura, "Effect of surface roughness on the statistical distribution of image speckle intensity," *Opt. Commun.* **11**, 35–38 (1974).
- H. Fujii and T. Asakura, "Statistical properties of image speckle patterns in partially coherent light," *Nouv. Rev. Opt.* **6**, 5–14 (1975).
- E. Jakeman and J. G. McWhirter, "Non-Gaussian scattering by a random phase screen," *Appl. Phys. B* **26**, 125–131 (1981).
- E. Jakeman, "Speckle statistics with a small number of scatterers," *Opt. Eng.* **23**, 234453 (1984).
- H. M. Pedersen, "The roughness dependence of partially developed, monochromatic speckle patterns," *Opt. Commun.* **12**, 156–159 (1974).
- K. A. O'Donnell, "Speckle statistics of doubly scattered light," *J. Opt. Soc. Am.* **72**, 1459–1463 (1982).
- S. Pau, S. N. Dixit, and D. Eimerl, "Electro-optic control of correlations in speckle statistics," *J. Opt. Soc. Am. B* **11**, 1498–1503 (1994).
- S. Kubota and J. W. Goodman, "Very efficient speckle contrast reduction realized by moving diffuser device," *Appl. Opt.* **49**, 4385–4391 (2010).
- D. Li, D. P. Kelly, and J. T. Sheridan, "K speckle: space-time correlation function of doubly scattered light in an imaging system," *J. Opt. Soc. Am. A* **30**, 969–978 (2013).
- Y. Bromberg and H. Cao, "Generating non-Rayleigh speckles with tailored intensity statistics," *Phys. Rev. Lett.* **112**, 213904 (2014).
- R. Fischer, I. Vidal, D. Gilboa, R. R. B. Correia, A. C. Ribeiro-Teixeira, S. D. Prado, J. Hickman, and Y. Silberberg, "Light with tunable non-Markovian phase imprint," *Phys. Rev. Lett.* **115**, 073901 (2015).
- J. P. Amaral, E. J. S. Fonseca, and A. J. Jesus-Silva, "Tailoring speckles with Weibull intensity statistics," *Phys. Rev. A* **92**, 063851 (2015).
- H. E. Kondakci, A. Szameit, A. F. Abouraddy, D. N. Christodoulides, and B. E. A. Saleh, "Sub-thermal to super-thermal light statistics from a disordered lattice via deterministic control of excitation symmetry," *Optica* **3**, 477–482 (2016).
- X. Li, Y. Tai, H. Li, J. Wang, H. Wang, and Z. Nie, "Generation of a super-Rayleigh speckle field via a spatial light modulator," *Appl. Phys. B* **122**, 82 (2016).
- M. Guillon, B. C. Forget, A. J. Foust, V. De Sars, M. Ritsch-Marte, and V. Emiliani, "Vortex-free phase profiles for uniform patterning with computer-generated holography," *Opt. Express* **25**, 12640–12652 (2017).
- S. Akbar, R. Fickler, M. J. Padgett, and R. W. Boyd, "Generation of caustics and rogue waves from nonlinear instability," *Phys. Rev. Lett.* **119**, 203901 (2017).
- C. Ventalon and J. Mertz, "Dynamic speckle illumination microscopy with translated versus randomized speckle patterns," *Opt. Lett.* **14**, 7198–7209 (2006).
- J. Gateau, T. Chaigne, O. Katz, S. Gigan, and E. Bossy, "Improving visibility in photoacoustic imaging using dynamic speckle illumination," *Opt. Lett.* **38**, 5188–5191 (2013).
- J.-E. Oh, Y.-W. Cho, G. Scarcelli, and Y.-H. Kim, "Sub-Rayleigh imaging via speckle illumination," *Opt. Lett.* **38**, 682–684 (2013).
- T. Chaigne, J. Gateau, M. Allain, O. Katz, S. Gigan, A. Sentenac, and E. Bossy, "Super-resolution photoacoustic fluctuation imaging with multiple speckle illumination," *Optica* **3**, 54–57 (2016).
- E.-F. Zhang, W.-T. Liu, and P.-X. Chen, "Ghost imaging with non-negative exponential speckle patterns," *J. Opt.* **17**, 085602 (2015).
- K. Kuplicki and K. W. C. Chan, "High-order ghost imaging using non-Rayleigh speckle sources," *Opt. Express* **24**, 26766–26776 (2016).
- S. Zhang, W. Wang, R. Yu, and X. Yang, "High-order correlation of non-Rayleigh speckle fields and its application in super-resolution imaging," *Laser Phys.* **26**, 055007 (2016).
- F. Jendrzejewski, A. Bernard, K. Müller, P. Cheinet, V. Josse, M. Piraud, L. Pezzé, L. Sanchez-Palencia, A. Aspect, and P. Bouyer, "Three-dimensional localization of ultracold atoms in an optical disordered potential," *Nat. Phys.* **8**, 398–403 (2012).
- K. Dholakia and T. Čížmár, "Shaping the future of manipulation," *Nat. Photonics* **5**, 335–342 (2011).
- G. Volpe, L. Kurz, A. Callegari, G. Volpe, and S. Gigan, "Speckle optical tweezers: micromanipulation with random light fields," *Opt. Express* **22**, 18159–18167 (2014).
- G. Volpe, G. Volpe, and S. Gigan, "Brownian motion in a speckle light field: tunable anomalous diffusion and selective optical manipulation," *Sci. Rep.* **4**, 3936 (2014).
- J. Bewerunge and S. U. Egelhaaf, "Experimental creation and characterization of random potential-energy landscapes exploiting speckle patterns," *Phys. Rev. A* **93**, 013806 (2016).
- K. M. Douglass, S. Sukhov, and A. Dogariu, "Superdiffusion in optically controlled active media," *Nat. Photonics* **6**, 834–837 (2012).
- C. Bechinger, R. Di Leonardo, H. Löwen, C. Reichhardt, G. Volpe, and G. Volpe, "Active particles in complex and crowded environments," *Rev. Mod. Phys.* **88**, 045006 (2016).
- E. Piñe, S. K. Velu, A. Callegari, P. Elahi, S. Gigan, G. Volpe, and G. Volpe, "Disorder-mediated crowd control in an active matter system," *Nat. Commun.* **7**, 10907 (2016).
- R. W. Gerchberg and O. W. Saxton, "A practical algorithm for the determination of the phase from image and diffraction plane pictures," *Optik* **35**, 237–246 (1972).
- M. Reicherter, T. Haist, E. U. Wagemann, and H. J. Tiziani, "Optical particle trapping with computer-generated holograms written on a liquid-crystal display," *Opt. Lett.* **24**, 608–610 (1999).
- S. M. Popoff, G. Lerosey, R. Carminati, M. Fink, A. C. Boccara, and S. Gigan, "Measuring the transmission matrix in optics: an approach to the study and control of light propagation in disordered media," *Phys. Rev. Lett.* **104**, 100601 (2010).
- J. Yoon, K. Lee, J. Park, and Y. Park, "Measuring optical transmission matrices by wavefront shaping," *Opt. Express* **23**, 10158–10167 (2015).
- C. W. Hsu, S. F. Liew, A. Goetschy, H. Cao, and A. D. Stone, "Correlation-enhanced control of wave focusing in disordered media," *Nat. Phys.* **13**, 497–502 (2017).
- S. G. Johnson, "The NLOpt nonlinear-optimization package," 2011, <http://ab-initio.mit.edu/nlopt>. We use the low-storage BFGS algorithm, which converges to the target pattern within 10,000 iterations: with an error less than 10%. The intensity PDF of the obtained pattern is the same as that of the target pattern.
- J. Nocedal, "Updating quasi-Newton matrices with limited storage," *Math. Comp.* **35**, 773–782 (1980).